



## Use of Circumferentially Cracked Bar sample for CTOD fracture toughness determination in the upper shelf regime

D. Gentile, I. Persechino, N. Bonora

*University of Cassino and Southern Lazio*

*gentile@unicas.it, i.persechino@unicas.it, nbonora@unicas.it*

G. Iannitti

*TECHDYN Engineering srl*

*g.iannitti@techdyn.it*

A. Carlucci

*SAIPEM S.A.*

*antonio.carlucci@saipem.com*

---

**ABSTRACT.** In this work, the use of circumferentially cracked bar (CCB) sample to determine material fracture toughness in the upper shelf regime for carbon steels has been investigated. Since high fracture toughness materials are known to exhibit extensive crack tip blunting before ductile crack initiation, accurate specimen design is required to provide realistic fracture toughness measurement. Here, a CCB was designed to have similar loss of constraint as for SENT sample. Continuum damage mechanics was used to predict the occurrence of ductile crack initiation and propagation. Finite element analysis was performed to predict specimen response and to compare computed J-integral crack driving force with measured CTOD. Finally, experimental tests were performed on X65 carbon steel and the measured critical CTOD was compared with available fracture data obtained with SENT.

**KEYWORDS.** Circumferentially cracked bar; Fracture; CTOD; CDM.

---

### INTRODUCTION

The determination of material fracture toughness is coded in standards, such as ASTM E399. Design codes and material testing standards provide also the sample geometry for fracture toughness determination. Although, crack driving force solutions for a number of possible alternative geometries are available, compact tension (CT), single edge crack in tension (SENT) or in bending (SENB) are usually recommended. For instance, the latter two geometries are recommended in DNV-OS-F101 standard for structural integrity assessment of subsea pipelines because they are characterized by geometry loss of constraint similar to that occurring in pipe welds circumferential flaws.

---



In engineering practice, the use of CT, SEN or SENT is not always practicable especially when material availability is limited. This is the case of multi materials joints, such as bi-metallic girth welds, where the amount of each material is insufficient to machine even small size fracture samples.

A possible alternative is given by the circumferential cracked bar (CCB) sample. This geometry is particularly simple in the design, it can be scaled according to the material availability, and it is free of three-dimensional effects because of radial symmetry. The idea of CCB as alternative fracture mechanics samples is not new. Notched cracked bar have been used by Stark and Ibrahim [1], Ibrahim and Stark [2-3], and Lam and Ibrahim [4]. Devaux et al [5] used axisymmetric cracked bar to determine local approach fracture parameters to compare with CT data. Beremin [6] used CCB to predict the condition for initiation and stable crack growth in low alloy steels. Giovanola and Crocker [7] performed a study aimed to demonstrate the possibility to measure representative fracture toughness for nuclear pressure vessel materials using small cracked round bars at different temperatures. They found, over the entire temperature range, a good agreement between fracture toughness values measured with CCB and 1T-CT for both cleavage and ductile fracture. Among the advantages offered by the CCB sample, they pointed out the possibility to achieve, under fully plastic regimes, a high degree of constraint at the crack tip even for small uncracked ligament and its use for the determination of the dynamic fracture toughness with split Hopkinson pressure bar [8-10]. The same year, Scibetta et al. [11] investigated computationally the loss of constraint in CCB sample in order to derive the conditions and specimen requirements for a valid measurement of plane strain fracture toughness.

Reviewed papers in the literature, mainly address the possibility to use circumferential cracked bar as alternative to measure fracture toughness in the lower shelf regime. Authors used axisymmetric bar geometry differing in the notch or crack shape. Most of them used V-notch while other used crack emanating from round notch. However, all of them agreed in using  $K_I$  or  $J_I$  as governing fracture parameters and this requires necessarily the use of finite element simulation for the determination of the effective crack driving force as a function of geometry parameters (i.e. crack depth ration, sample height, etc.) and applied load. For instance, Wang et al. [12] reported the following  $K_I$  solution for V-notch circumferentially cracked bar under remote tension,

$$K_I = 0.932 \frac{P\sqrt{D}}{d^2\sqrt{\pi}} \text{ for } 1.2 \leq D/d \leq 2.1 \quad (1)$$

where  $D$  is the remote bar diameter,  $d$  is the minimum diameter at the V-notch, and  $P$  the maximum load. Such general solutions based on FEM analysis, depends on a number of computational issues. These includes the material model (elastic or elastic-plastic), the implementation of strain energy release method for contour integral determination, as well as other computational issues (element type, large or small strain formulations, etc.) inherently related to the code used at the time the simulation was performed. Bonora et al. [10], proposed the use of CCB to determine material resistance using the critical crack tip opening displacement (CTOD,  $\delta_c$ ) as fracture parameter. They highlighted the possibility offered by such sample geometry to directly measure the material resistance using either the digital image correlation (DIC) technique or alternatively, a high speed video camera avoiding numerical simulation or to refer to not well assessed analytical solutions. Using well-known relationships between the CTOD and  $K_I$  and  $J_I$ , material fracture resistance in the lower and upper shelf regime can be easily determined.

The scope of this work was to investigate the use of CCB to determine fracture resistance of high toughness materials in the upper shelf regime. This task poses a number of complexities since these materials are known to show extensive blunting before ductile tearing initiation and propagation in association with substantial loss of constraint. In axisymmetric bar, the development of an extensive crack tip blunting may cause the flaw to behave like a notch and not like a crack triggering ductile failure in the center of the uncracked ligament. In addition, an excessive loss of constraint may lead to fracture toughness values which differs significantly from those measured in other geometries such as CT. Therefore, an accurate design of CCB is required to provide realistic fracture strength measurement.

## SEN(T) AND CCB(T) ANALYSIS IN THE J-Q SPACE

In design codes and standards for oil and gas application, as in OS-DNV-F101, the use of SENT is recommended for the experimental determination of the material critical crack tip opening displacement. From the design standpoint, outer circumferential weld crack subjected to remote axial strain loading, is one flaw configuration of major concern. Loss of constraint in SENT is similar to that occurring for this crack configuration in welded joints. Although SENT sample is relatively easy to be extracted for the base metal in the longitudinal direction of the pipe, it is often difficult or

impossible to machine this sample geometry for girth weld or base metal along the circumferential direction. Situation becomes even more complicated when dealing with the corrosion resistant alloy (CRA) layer in clad pipe. In this case, 4 mm is a typical thickness for the clad and therefore it is impracticable to machine a SENT sample with such limited material availability.

Specimen geometry, as well as crack depth ratio, has an effect on measured fracture toughness. A loss of constraint, resulting from large-scale yielding, relaxes the stress concentration for notched-tension panels and shallow-notch specimens, while deep-notch bend and compact specimens maintain a high level of crack tip constraint. This leads to an apparently increased fracture resistance in term of  $K_{Ic}$ ,  $J_{Ic}$  and  $\delta_c^*$  for the former configurations [13, 14]. T-stress and Q-parameter - respectively in the K and J-controlled stress fields - have been proposed to characterize the constraint effect on the crack tip. The T-stress and Q-parameter at fracture are not material constants but depend on specimen geometry of specimens. Since the objective of the work was the investigation of the CCB sample for the determination of fracture toughness in the upper shelf regime, the Q-parameters was selected to characterize the constraint. An extensive finite element simulation analysis was performed to determine the J-Q path in SENT and CCB for varying crack depth ratio to verify if similar constraint can be realized for these geometry samples. For each selected crack depth ratio, the opening stress ( $\sigma_{yy}^{geom}$ ) along the crack ligament was extracted as a function of the applied J-integral value. Successively, a modified boundary layer (MBL) analysis was carried out inferring the same J-integral value and T-stress set to zero. Again, the opening stress ( $\sigma_{yy}^{MBL}$ ) along the ligament was extracted. Hence, the Q-stress was determined according to:

$$Q = \frac{\sigma_{yy}^{geom} - \sigma_{yy}^{MBL}}{\sigma_0} \quad (2)$$

Since the opening stress varies with the distance from the crack tip, the Q-stress was evaluated taking the stress field values at  $\theta = 0^\circ$  and  $r = 2J / \sigma_0$ , where  $\sigma_0$  is the reference material yield stress. Finite element simulations have been carried out with MSC MARC r2013 commercial FEM code using fully integrated four node elements with bilinear shape functions. All elastic-plastic simulations were performed using large displacement, Lagrangian updating and finite strain formulation. The J-integral was calculated using the domain integral formulation which ensures accurate estimation under general loading conditions. To account for extensive plastic zone development at the tip, an initial blunting was introduced in the FEM model.

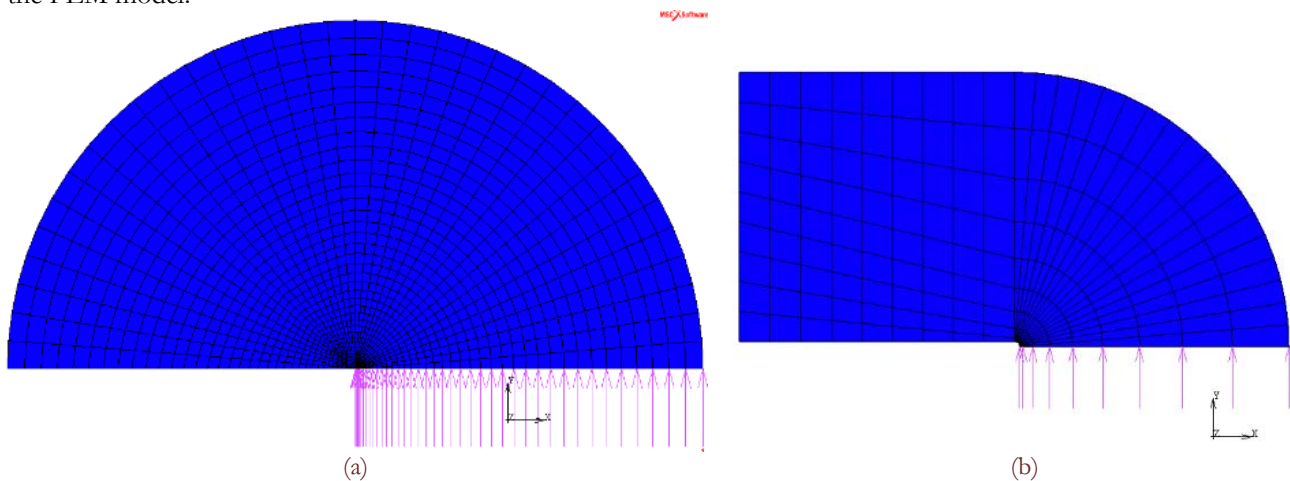


Figure 1: Finite element mesh for MBL: a) whole model, b) detail of the near tip region showing the initial crack blunting. Arrows indicates symmetry boundary conditions applied as constrained displacement to the nodes.

The initial blunt radius used in this work was  $r=0.01$  mm. This value is small enough to follow accurately the transition from the linear elastic to the elastic-plastic stress field. For both specimen and MBL model the same mesh was used. Boundary conditions were selected accordingly, Fig. 1. The minimum element size at the tip was 0.0063 mm. For both SENT and CCB, four crack depth ratios ( $a/W$  or  $a/R=0.2, 0.3, 0.4,$  and  $0.5$ ) have been investigated. Reference dimensions for the SENT were taken in accordance to [15]. For the CCB, there are no prescribed dimensions. For the purpose of the analysis, the mesh used for the CCB was the same as for SENT.

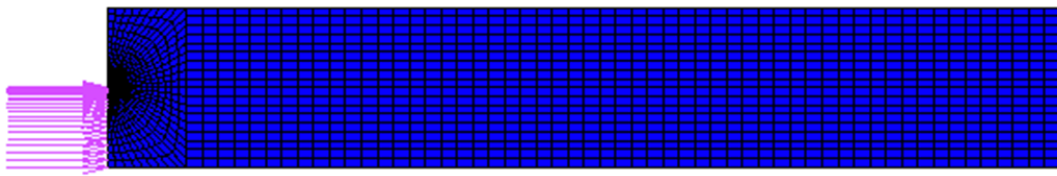


Figure 2: Finite element mesh for SENT and CCBT ( $a/W$  and  $a/R=0.5$ ). Same mesh but different element type: plane strain for SENT, axisymmetric for CCBT.

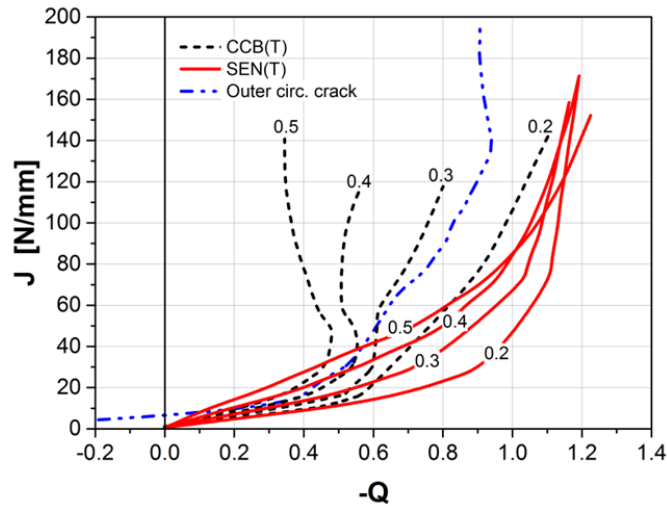


Figure 3: Comparison of the calculated J-Q paths for SENT and CCBT for different crack depth ratios. The J-Q path for a outer circumferential girth weld crack is also shown.

In Fig. 3 the summary of the calculated J vs -Q parameter for SENT and CCB. Is given. As anticipated, the Q-parameter does not remain constant for increasing J-integral values. For each crack depth ratio, a saturation Q value is reached for fully developed plastic zone. These results indicate that the loss of constraint in CCB is less severe than in SENT, in general. J-Q paths in SENT have the tendency to converge for high J-integral values, resulting in similar values independently on the crack depth ratio. CCB J-Q paths become steeper for deeper crack. However, it was found that in CCB shallow crack ( $a/R=0.2$ ) result in similar constraint as for SENT with  $a/W=0.5$ . In Fig. 3, the J-Q path for outer circumferential crack typically used in the Engineering Criticality Assessment (ECA) procedure is also plotted for comparison. Based on this, it was decided to use CCB  $a/R=0.2$  for investigating the critical CTOD in carbon steel and to compare with fracture toughness data obtained with SENT.

C	Si	Mn	P	S	Cr	Ni	Cu
0.091	0.4	1.37	0.009	0.0007	0.024	0.27	0.17

Table 1: Chemical composition of the C-Mn steel.

## MATERIAL

The material under investigation is C-Mn X65 pipe steel grade with the nominal composition given in Tab. 1. The material was fully characterized at RT and the flow curve was determined according to the procedure given in [10]. A two-term Voce law was used as,

$$\sigma = 601 + 38(1 - \exp(-\varepsilon_p / 0.012)) + 250(1 - \exp(-\varepsilon_p / 0.206)) \quad (3)$$

The measured flow stress was found to be higher than that expected for this steel grade. The nominal reference ductile-to-brittle transition temperature is  $-100^\circ\text{C}$ , consequently at RT the material is completely in the upper shelf regime.

## DUCTILE TEARING ANALYSIS

**D**uctile crack initiation and propagation analysis in CCB was performed using Bonora's damage model [16]. This model is derived in the framework of continuum damage mechanics and was verified for different classes of metals and alloys [17]. In this model, damage affects only the elastic stiffness while damage effects flow stress are taken into account in the definition of the material flow curve, leading to a non-softening formulation, which has the advantage to avoid mesh dependency of the solution. Here, damage accumulates only under positive (tensile) state of stress while in compression damage effects are temporarily restored. The model requires only four material parameters to be determined:  $\epsilon_{th}$  the threshold strain at which damage processes initiates;  $\epsilon_f$  the failure strain under constant uniaxial constant stress triaxiality;  $D_{cr}$ , the critical damage at rupture and the shape factor  $\alpha$ . These parameters are characteristic of the material and do not depend on the geometry [17].

The damage rate is given by the following expression,

$$\dot{D} = \alpha \cdot \frac{D_{cr}^{\frac{1}{\alpha}}}{\ln(\epsilon_f / \epsilon_{th})} \cdot R_v \cdot (D_{cr} - D)^{\frac{\alpha-1}{\alpha}} \cdot \frac{\dot{\epsilon}^p}{\epsilon^p} \quad (4)$$

The function  $R_v$  accounts for stress triaxiality effect,

$$R_v = \frac{2}{3}(1 + \nu) + 3 \cdot (1 - 2\nu) \cdot \left( \frac{\sigma_H}{\sigma_{eq}} \right)^2 \quad (5)$$

where  $\sigma_H$  is the pressure and  $\sigma_{eq}$  is the von Mises stress and  $\nu$  is the Poisson's ratio. For the material under investigation, damage model parameters have been determined according to the procedure described in [18] and summarized in Tab. 2. This procedure is based on fracture data, obtained from traction tests performed on smooth and round notched samples, and numerical simulation aimed to build the failure locus in terms of stress triaxiality vs average failure strain.

Threshold strain $\epsilon_{th}$	Failure strain $\epsilon_f$	Critical damage $D_{cr}$	$\alpha$
0.288	4.15	0.1	0.3

Table 2: Summary damage model parameters.

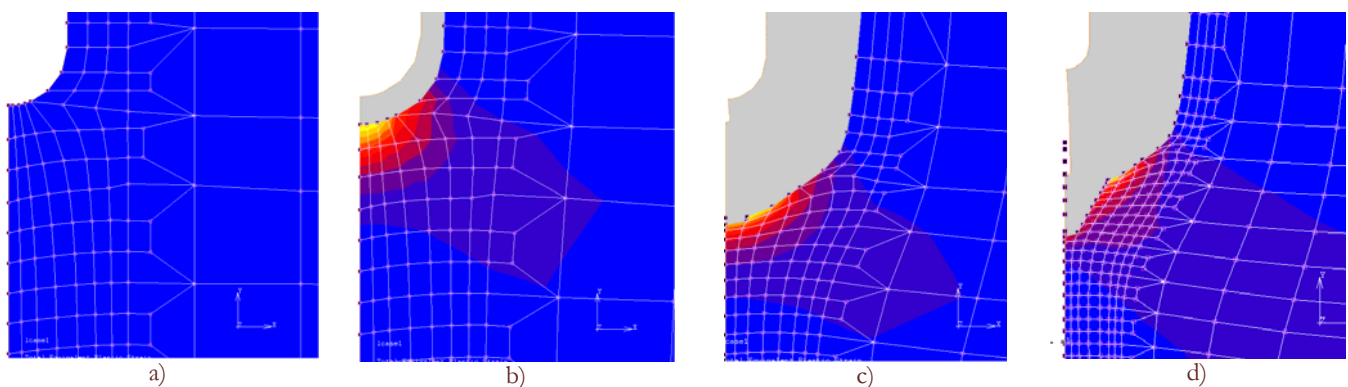


Figure 4: Evolution of damage development at the crack tip of CCB  $a/R=0.2$  under remote tension load: a) initial configuration; b) blunting development; c) crack initiation; d) crack propagation.



Finite element analyses were performed with MSC MARC 2013r1 in which the Bonora's damage model is available. Numerical simulation of CCB incorporating damage was performed using the same computational parameters discussed in the previous paragraph. Crack propagation was simulated using element removal technique: when the damage reaches its critical value at the element first Gauss point, the element is removed and the stress and strain are set to zero. Although the damage model formulation does not suffer mesh size dependence, the size of the element has direct influence on the crack growth rate. As rule of thumb, the minimum element size should not be smaller than the material average grain size. In Fig. 5 the sequence of the deformation and damage development at the crack tip for the CCB  $a/R=0.2$  is shown. This result showed that, although extensive blunting occurs at the tip prior tearing initiation, crack propagation starts at the tip and propagates along the ligament confirming that the blunted crack still behaves as a "crack". Numerical simulation have been repeated simulating partial unloading at prescribed remote imposed displacement in order to evaluate the change in the unloading compliance as a function of crack advance. This result was used to validate damage simulation comparing with predicted crack growth with experimental data.

### CCB DESIGN AND EXPERIMENTAL TESTING

Based on computational analyses results, the geometry given in Fig. 5, for the CCB was selected. The remote diameter was 6.0 mm, the crack depth ratio was 0.2 and the longitudinal gauge length was  $L=30$  mm. The circumferential crack was machined using EDM and no fatigue pre-cracking was prescribed. The nominal notch radius was 0.06 mm. For testing in the upper shelf regime, this value is small enough to be considered as a sharp crack.

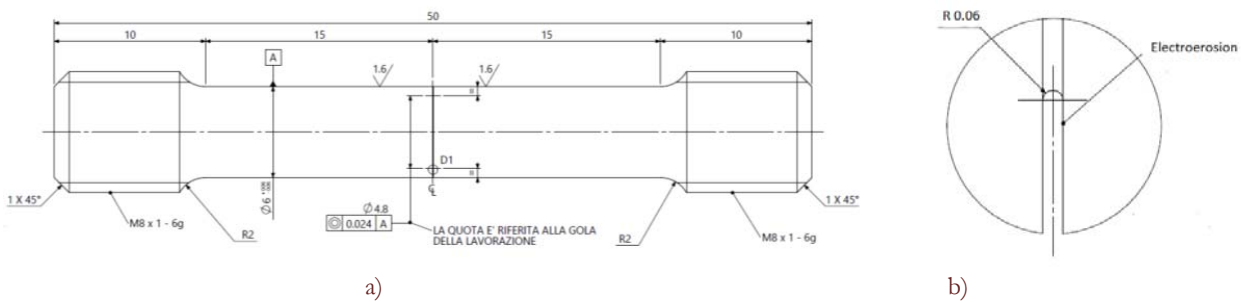


Figure 5: a) CCB dimensions, b) detail of the crack tip.

Specimen ends where thread in order to avoid slip during loading. Four samples were machined and their effective dimensions are summarized in Tab. 3. Of the four samples, two were monotonically loaded in tension up to failure while the other two were used for damage assessment performing partial unloading at prescribed remote imposed displacements. Elongation was measured using an extensometer with a reference length of 12.5 mm. Additionally, strain was measured using DIC. High speed video camera was used to monitor crack tip blunting development and first crack initiation for CTOD determination. In Fig. 6 the CCB instrumented with the clip gauge is shown. In Fig. 7 a sequence of crack blunting development observed with the video camera is given.

Specimen	Outer diameter (mm)	Minimum diameter (mm)	EDM notch radius (mm)
CCB_B1	5.993	4.814	0.0595
CCB_B2	6.014	4.826	0.0605
CCB_B3	6.004	4.797	0.0590
CCB_B4	6.026	4.812	0.0610

Table 3: Specimen dimension. Tensile test.



Figure 6: Reference set-up for CCB.

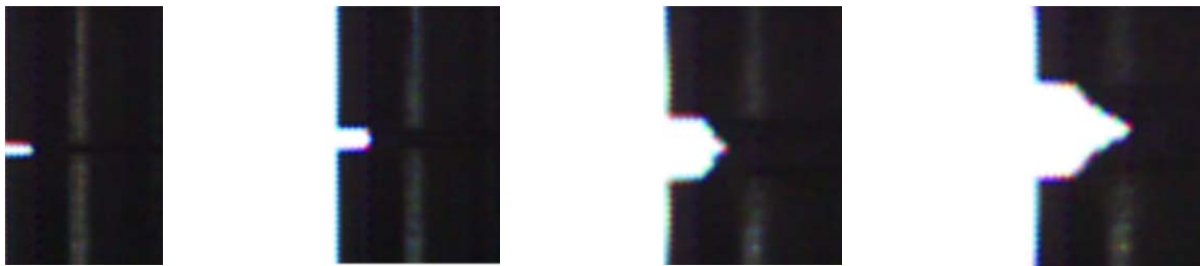


Figure 7: Sequence of crack tip blunting development and crack initiation observed with high speed camera.

## RESULTS AND DISCUSSION

For each test, the global response in terms of applied load vs elongation was recorded while the CTOD at crack initiation was derived from the video recording. Tests showed that crack initiation occurred beyond the maximum load indicating that some sort of necking develops in the minimum section. This was indeed confirmed by the video recording of the test and later verified also by FEM analysis. In Fig. 8, the comparison of the measured applied load vs average strain (from extensometer) and calculated response with FEM is shown. Here, it can be observed that specimens CRB\_B1, that was monotonically loaded up to fracture, and CRB\_B4, that was subjected to partial unloading, showed very similar responses. Some differences were observed in specimen CRB\_B2 that showed a higher yield stress and more rapid load drop beyond maximum load. Finite element simulation results were in a general good agreement with the experimental data although the calculated response was in a better agreement with that of CRB\_B2 sample.

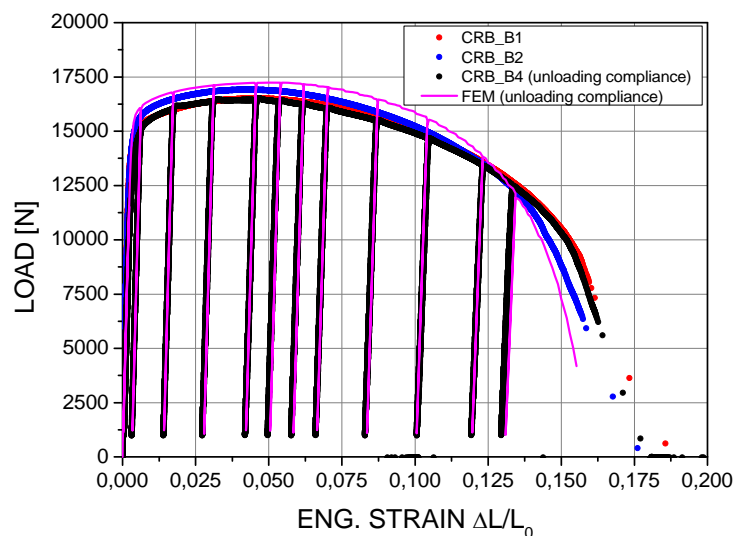


Figure 8: Comparison of applied load vs strain response measured in the tests and predicted with FEM.



Crack propagation as a function applied load was also compared with finite element prediction obtained with the damage model. In Fig. 9, the comparison is given. Here, experimental crack advance data have been obtained from the high speed camera filming. Again the comparison with computational results is in a general good agreement considering that simulation have been performed using model parameters identified on different test types. The comparison is quite good up to 0.6 mm of crack advance that correspond to a crack depth ratio of 0.4. For larger crack advance the difference between the predicted and the measured response increases. This is probably due to the fact the FEM do not reproduce accurately the global response in the final part of the load vs strain curve as shown in Fig. 8.

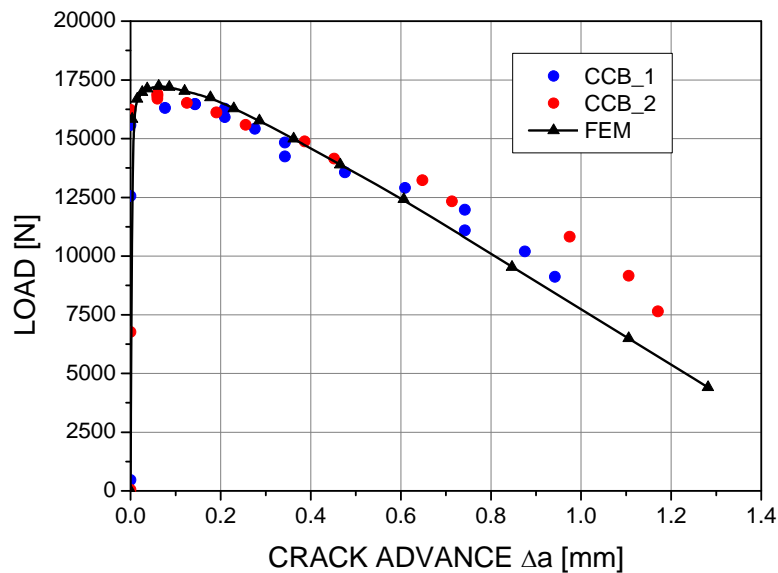


Figure 9: Comparison of predicted and measured applied load vs crack advance.

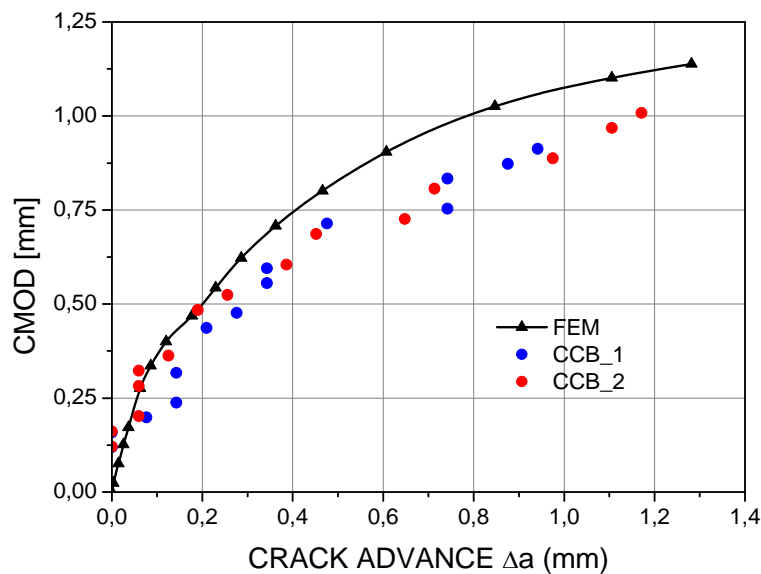


Figure 10: Comparison of predicted and measured CMOD vs crack advance.

Similar agreement was found for the crack mouth opening displacement (CMOD) vs crack advance response, Fig. 10. Finally, results in terms of crack resistance curve were also provided. From the computational point of view, the J-integral was calculated using the domain integral formulation available in MSC MARC while the applied J-integral in the experiment was estimated using the relationship provided in [19].

$$J = \frac{1}{(2\pi r_0^2)} \left[ 3 \int_0^{\delta_{cr}} P d\delta_{cr} - P \delta_{cr} \right] \quad (6)$$

where  $P$  is the applied load,  $\delta_{cr}$  is the load point displacement which is function of the compliance of the uncracked specimen, and  $r_0$  is the uncracked ligament. Results are provided in Fig. 11.

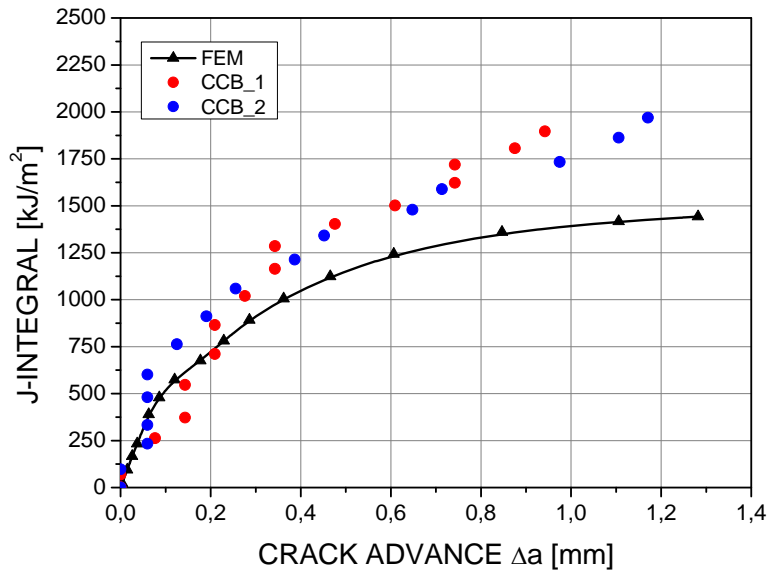


Figure 11: Comparison of calculated crack resistance and crack driving force obtained using unloading compliance values.

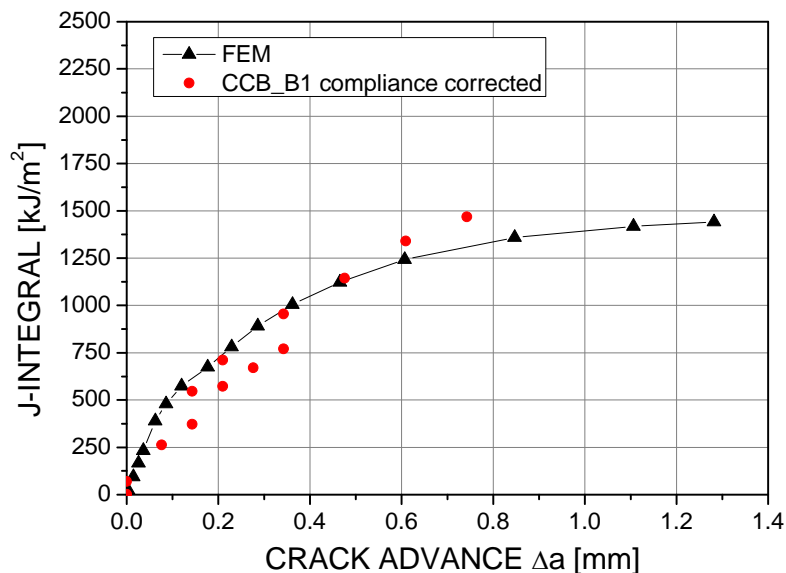


Figure 12: Crack resistance curve calculated considering the change in the unloading compliance.

It can be seen that the agreement is good up to J-integral values of  $\sim 600$  N/mm, which correspond to the maximum load. This is coherent with Eq. (6) that is valid up to the maximum load. Beyond this point, Eq. (6) shall be corrected considering the change in the unloading compliance due to crack advance. Therefore, crack resistance data have been recalculated using the unloading compliance measured in the tests. The new crack resistance curve is shown in Fig. 12. This time, a better agreement between the experimental values and the FEM results is found up to  $\sim 1.0$  mm of crack growth.



Specimen	CTOD Max load [mm]	CTOD FEM Max load [mm]	Critical CTOD ( $\Delta a=0.1$ mm) [mm]	CTOD FEM ( $\Delta a=0.1$ mm) [mm]
CCB_B1	0.489	0.380	0.879	0.56
CCB_B2	0.458	0.380	0.784	0.56
CCB_B3	0.394	0.380	0.788	0.56
CCB_B4	0.365	0.380	0.852	0.56
SENT (a/W=0.5)	0.460	0.40	-	-

Table 4: Summary of CTOD measurement for CCB and SENT.

Finally, the CTOD measured in the tests was compared with data obtained on SENT [20]. CTOD for SENT was measured, after cutting and polishing on an interrupted test at maximum load. This value is usually considered as design allowable in several design codes. In Tab. 4, the summary of the CTOD at maximum load are given. In the Table the estimated critical CTOD for which crack propagation has occurred is given. The resolution of video recording is such that the crack advance can be estimated with a sensitivity of  $\pm 0.1$  mm since this is the size of the pixel. The CTOD at maximum load for CCB was  $0.426 \pm 0.057$  mm that is in a good agreement with the value measured for SENT, while the estimated critical CTOD for a minimum of 0.1 mm crack advance was  $0.826 \pm 0.047$  mm. The CTOD at maximum load estimated with FEM is in a very good agreement with the experimental data. On the contrary, the CTOD for 0.1 mm of crack advance, is 30% less than the experimental measure. Probably, this can be explained by the variability of the material plastic flow curve, which is also responsible for the differences observed in the predicted applied load vs elongation curve.

## CONCLUSIONS

In this work, the use of the circumferentially cracked bar sample to determine the CTOD fracture toughness in the upper shelf regime, has been investigated. Based on finite element simulation, the CCB crack depth ratio that exhibits the same Q-parameter as for SENT with a/W=0.5, was found a/R=0.2. It was verified that with such crack depth ratio, considering the extensive blunting occurring at the tip, the flaw in CCB still behaves as a crack (that is ductile tearing always occurs at the tip). Experimental tests performed at RT on X65 carbon steel grade, showed CTOD values in a very good agreement with that measured using standard SENT geometry sample confirming the equivalence of CCB with SENT. The critical CTOD for 0.1 mm crack advance was found twice that at maximum load which is usually indicated as allowable value in the design practice. Predictions performed with damage mechanics have been found to be in a very good agreement with experimental finding indicating that this approach is a mature tool for preliminary analysis and design of experiment in order to anticipate expected material/geometry behaviour and to reduce the experimental effort.

## REFERENCES

- [1] Stark H. L., Ibrahim, R. N., Estimating fracture toughness from small specimens, *Engineering Fracture Mechanics*, 25 (1986) 395-401.
- [2] Ibrahim R. N., Stark, H. L., Validity requirements for fracture toughness measurements obtained from small circumferentially notched cylindrical specimens, *Engineering Fracture Mechanics*, 28 (1987) 455-460.
- [3] Ibrahim R. N., Stark, H. L., Establishing K1c from eccentrically fatigue cracked small circumferentially grooved cylindrical specimens, *Int. J. of Fracture* 44, 179-188 (1990).
- [4] Lam Y. C., Ibrahim, R. N., Improvement of the Fracture Toughness of an Aluminum Alloy, *Fatigue Fract. Engng. Mater. Struct.* 17 (1994) 277-284.
- [5] Devaux, J. C., Rousselier, G., Mudry, F., Pineau, A., An experimental program for the validation of local ductile fracture criteria using axisymmetrically cracked bars and compact tension specimens, *Engineering Fracture Mechanics*, 21 (1985) 273-283.



- [6] Beremin, F. M., Calculation and experiment on axisymmetrically cracked tensile bars: prediction of initiation, stable crack growth and instability, In: Transactions of the 6th Int. Conference on Structural Mechanics in Reactor Technology, L (1981) L 6/2.
- [7] Giovanola, J. H., Crocker, J. E., Fracture toughness testing with cracked round bars: feasibility study, NUREG/CR-6342 ORNL/SUB/94-DHK60, US Nuclear Regulatory Commission, Washington DC, (2000).
- [8] Costin, L. S., Duffy, J., Freund, L. B., Fracture initiation in metals under stress wave loading conditions, In: Fast Fracture and Crack Arrest, ASTM STP 62 7, G. T. Hahn and M. F. Kanninen, Eds., American Society for Testing and Materials, Philadelphia, (1977) 301-318
- [9] Hawley, R. H., Duffy, J., Shih, C. F., Dynamic notched round bar testing, In: ASM Metals Handbook, 9th ed., Mechanical Testing, American Society for Metals, Metals Park, Ohio, 8 (1985) 275-282.
- [10] Bonora, N., Ruggiero, A., Testa, G., Iannitti, G. and Gentile, D., Dynamic Crack Tip Opening Displacement (DCTOD) as governing parameters for material fragmentation, J. of Physics: Conference Series, 500(11) (2014).
- [11] Scibetta, M., Chaouadi R., Van Walle, E., Fracture toughness analysis of circumferentially-cracked round bars, Int. J. of Fracture, 104 (2000) 145-168.
- [12] Wang, C.H., Introduction to Fracture Mechanics; Stress analysis of cracked bodies, Aeronautical and Maritime Research Laboratory, Victoria 3001, Melbourne, DSTO-GD-0103, (1996) 10-28.
- [13] Minami, F., Inoue, T., Arimochi, K., Constraint correction of fracture toughness CTOD for fracture performance evaluation of structural components, In: 10th Int. Conference on Fracture ICF10 Elsevier Science, Honolulu, Hawaii, USA, 2001 (1-6).
- [14] Betegòn, C., Hancock, J. W., Two parameter characterization of elastic-plastic crack tip fields, J. of Applied Mechanics, 58 (1991) 104-110.
- [15] DNV-OS-F101, Offshore Standard - Submarine Pipeline Systems, (2012) 1-367.
- [16] Bonora, N., A non-linear CDM damage model for ductile failure, Engineering Fracture Mechanics, 58(1/2) (1997) 11-28
- [17] Bonora, N., Ruggiero, A., Esposito, L., Gentile, D., CDM modeling of ductile failure in ferritic steels: assessment of the geometry transferability of model parameters, Int. J. of Plasticity, 22(11) (2006) 2015-2047.
- [18] Carlucci, A., Bonora, N., Ruggiero, A., Iannitti, G., Crack initiation and growth in bimetallic girth welds, In: Proc. Proceedings of the ASME 2014, 33rd Int. Conference on Ocean, Offshore, and Arctic Engineering - OMAE 2014, ed. ASME, (2014) 1-5.
- [19] Giovanola J. H., Kobayashi, T., Mechanics of Deformation and Ductile Tearing in Cracked Round Bar Specimens, Engineering Fracture Mech., 59(2) (1998) 117-136.
- [20] Carlucci, A., Bonora, N., Ruggiero, A., Iannitti, G., Testa, G., Crack initiation and propagation of clad pipe girth weld flaws, In: Proc. of ASME 2014 Pressure Vessel and Piping Division Conference, PVP201, (2014) 28017.